Organic Electronics 83 (2020) 105777

Contents lists available at ScienceDirect

Organic Electronics

journal homepage: http://www.elsevier.com/locate/orgel

Solution-processed self-assemble engineering PDI derivative polymorphisms with optoelectrical property tuning in organic field-effect transistors

Xitong Liu [a], Haixiao Xu [a], Yecheng Zhou [b], Canglei Yang [a], Guangfeng Liu [c], Lixing Luo [a], Wei Wang [a], Yudong Ma [a], Jianqun Jin [a], Jing Zhang [a,*], Wei Huang [a]

[a] Key Laboratory for Organic Electronics and Information Displays & Jiangsu Key Laboratory for Biosensors, Institute of Advanced Materials (IAM), Jiangsu National Synergetic Innovation Center for Advanced Materials, Nanjing University of Posts & Telecommunications, 9 Wenyuan Road, Nanjing, 210023, China
[b] School of Materials Science & Engineering, Sun Yat-Sen University, Guangzhou, 510275, Guangdong, PR China
[c] Department of Chemistry, Uniwersitcé Libre de Bruxelles, Avenue F. D. Roosevelt 50, 1050, Brussels, Belgium

ARTICLE INFO

Keywords:
PDI derivative
Polymorphisms
Intermolecular interaction
Electron transport
Photo-response
Structure-property relationship

ABSTRACT

The crystal polymorphism study leads to an explosion of science research, related to many fields, such as organic semiconductors, pharmaceuticals, pigments, food, and explosives. Two different crystal phases of a perylene diimide derivative (4FPEPTC) have been prepared via a simple and efficient solution method. Via changing the concentration of the solution, we observed the polymorphisms clearly, wire-shape (α phase) and ribbon-like (β phase) crystals differed in the stacking mode and short-contacts. Moreover, the as-prepared *n*-channel microcrystal-based devices demonstrated distinct electron mobilities that of α phase architecture higher than β phase structure and obvious photoresponse discrepancy. Theoretical calculations further confirmed this phenomena, which help us to understand the structure-property relationship in this crystal polymorph. Our study indicates that the investigation of polymorphisms could be considered as a very useful method to realize functional property modulation and benefits the development of organic (opto)electronics.

1. Introduction

The evolution of organic semiconductors (OSCs) received great interests for their applications in optoelectronic devices and flexible electronics as an ideal replacement of inorganic counterparts in these years [1,2]. High performances have been achieved through the organic active layer construction. However, the physical and electronic properties [3] are highly related to the molecular inner stacking structure besides the chemical structure [4–9]. Owing to the weak non-bonding intermolecular interactions existed in the organic molecules, it is quite possible for the researchers to regulate semiconductor aggregation to crystallize into various packing arrangements [10–12]. Thus different polymorphs are supposed to possess distinct physical properties [13,14] attracting considerable research attentions [5,9,15–17]. For instance, pentacene [18,19], rubrene [20,21] and tetrathiafulvalenes [22] has been reported to manifest phase-depended charge carrier mobilities [23]. Even delicate changes in the intermolecular packing in crystalline molecular semiconductors can therefore tremendously impact intermolecular electronic coupling and substantially influence charge transport [24–28]. Polymorphism exploration plays an important role in organic electronics [29]. First, it is used as an avenue for enhancing the device performance without changing the chemical structure and, second, it is used as an ideal platform for examining the fundamental relationships between charge transport and crystal structure. Generally, polymorphic modifications exhibit different band structure, electron coupling, and electron phonon coupling, resulting in differences in charge transport behavior in organic field effect transistors (OFETs) [18,20,30,31].

Notably that the rational preparation of single crystal polymorphs using controllable molecular stacking arrangements has not been fully realized. On the one hand, the molecular conformations have a significant effect on the internal structure and symmetry of organic microcrystals [32]. On the other hand, organic microcrystals are held together by weak intermolecular interactions like van der Waals' force [10–12,33]. This makes the nucleation of organic microcrystals highly dependent on the outer environment conditions, including the kinds of

* Corresponding author.
E-mail address: iamjingzhang@njupt.edu.cn (J. Zhang).

https://doi.org/10.1016/j.orgel.2020.105777
Received 22 January 2020; Received in revised form 9 April 2020; Accepted 12 April 2020
Available online 18 April 2020

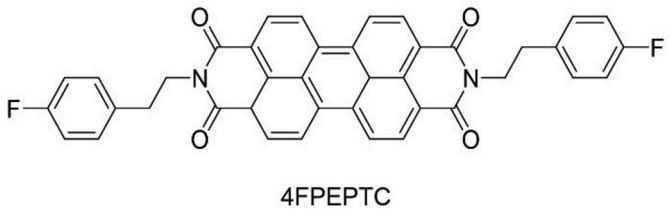

Scheme 1. Chemical Structure of 4FPEPTC.

solvents [34], temperature [35], solution concentration [5], and surfactants [36]. Therefore, kinetic control on the growth of different single-crystalline polymorphs for optimizing the optoelectronic properties remains a formidable task. Moreover, it still requires a lot to develop air-stable n-type materials and explore the influence of polymorphism on *n*-channel OFETs. Perylene tetracarboxylic diimides (PDIs) as the typical *n*-type OSC class have been widely investigated since first reported by Horowitz et al. [37] Fluorinated [38,39] and 1,7-Dicyano [40] derivatives exhibits excellent air stability and good performance owing to the deeper the lowest unoccupied molecular orbitals (LUMO) energy level to get rid of oxygen and water damage. Such unique F and O atom containing functional materials which could involving kinds of short contacts can act as good candidate to the supramolecular arrangement adjusting.

Herein, we demonstrate controllable solution self-assembly of two different crystal phases of a PDI derivative, N,N′-bis[2-(4-fluoro-phenyl)-ethyl]-3,4,9,10-perylenetetradicarboximide (4FPEPTC, Scheme 1). Through tuning the original solution concentrations, dynamically controlled formation of 4FPEPTC polymorphs was manipulated towards one-dimensional nanowires (1D-NWs) at 0.02 mg/ml and nanoribbons (NRs) at 0.2 mg/ml as the stable product. The standing manner of the *n*-type 4FPEPTC varied on the substrates for the weak-bond interactions change caused by the distinct arrangements. The nanoribbon-shaped β phase crystals displayed the highest electron mobility of 0.21 $cm^2 V^{-1} s^{-1}$ whereas the nanowire-shaped α phase crystals showed electron mobility up to 1.0 $cm^2 V^{-1} s^{-1}$, which is among the highest values for *n*-type organic semiconductors measured under ambient conditions. Meanwhile, the α phase framework revealed more drastic photoresponse behaviors as a result of the intrinsic arrangement variation.

2. Experimental

2.1. Materials

N,N′-bis[2-(4-fluoro-phenyl)-ethyl]-3,4,9,10-perylenetetradicarboximide (4FPEPTC) was purchased from Aldrich and employed without any purification.

2.2. Preparation of α and β phase crystals

The 4FPEPTC crystals were prepared using slow cooling method of saturated solutions at high temperature. Two 4FPEPTC chlorobenzene solutions with different concentration (0.02 mg/ml and 0.2 mg/ml) were heated at high temperature for complete dissolution. Then the resultant oversaturated solutions were naturally cooled under ambient conditions. Quantities of needle-like or ribbon-shaped crystals were observed on the bottom of the bottle after 1 or 2 days keeping.

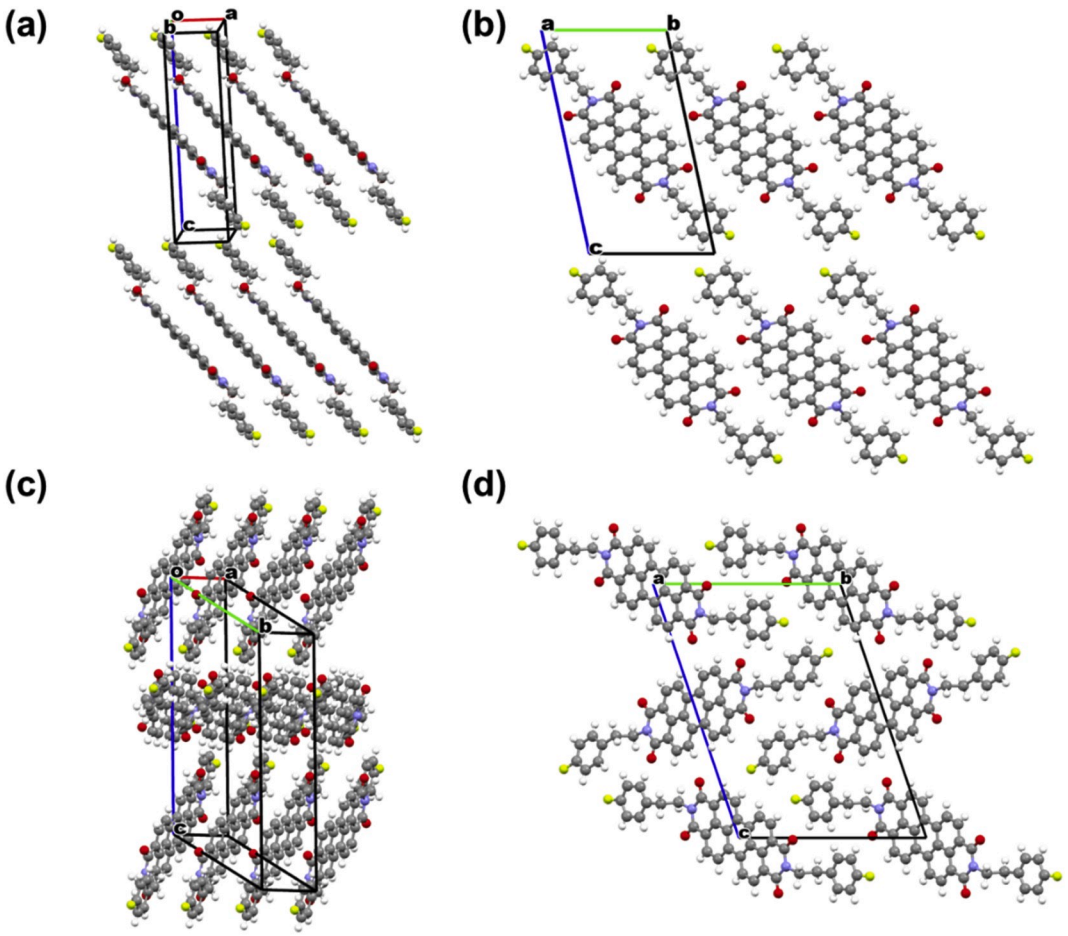

Fig. 1. Crystal structure of the 4FPEPTC crystals. Crystal packing and overlap pattern view along the *a*-axis of (a, b) α phase and (c, d) β phase structure.

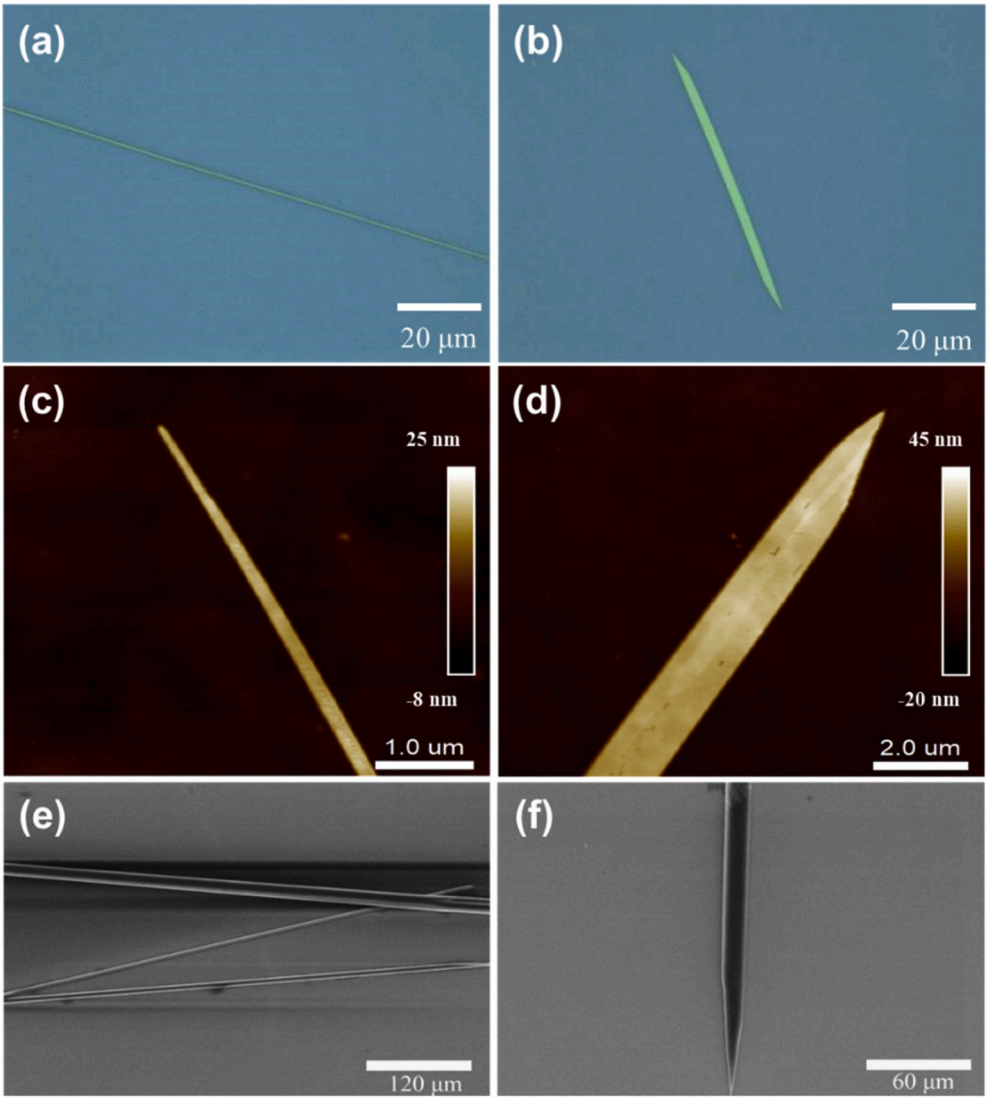

Fig. 2. Optical micrographs of the self-assembled (a) α phase and (b) β phase microcrystals and their (c, d) AFM and (e, f) SEM patterns.

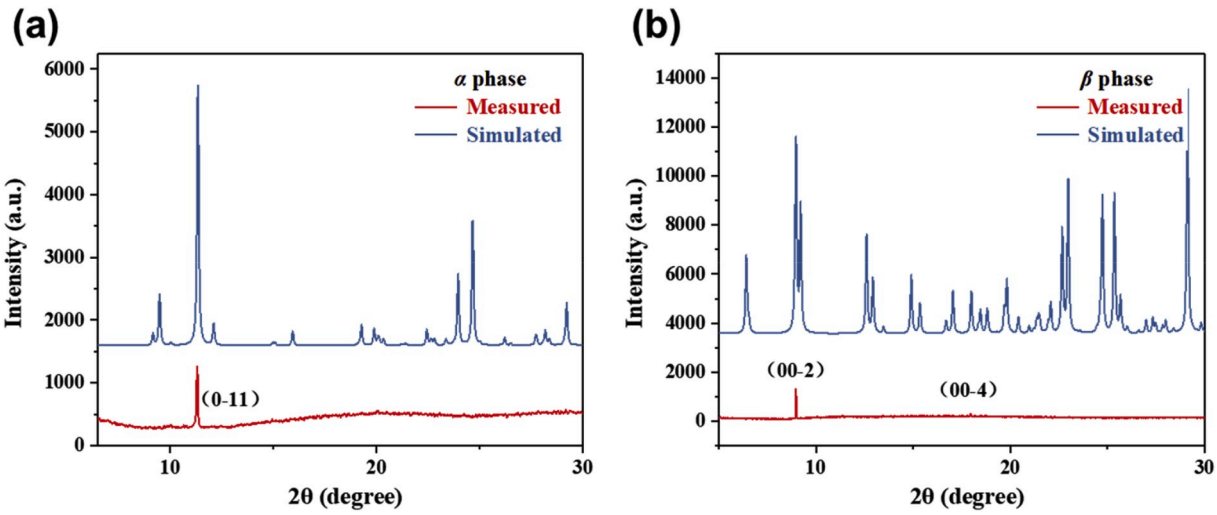

Fig. 3. Measured and simulated X-ray diffraction (XRD) patterns of (a) α phase and (b) β phase microcrystals.

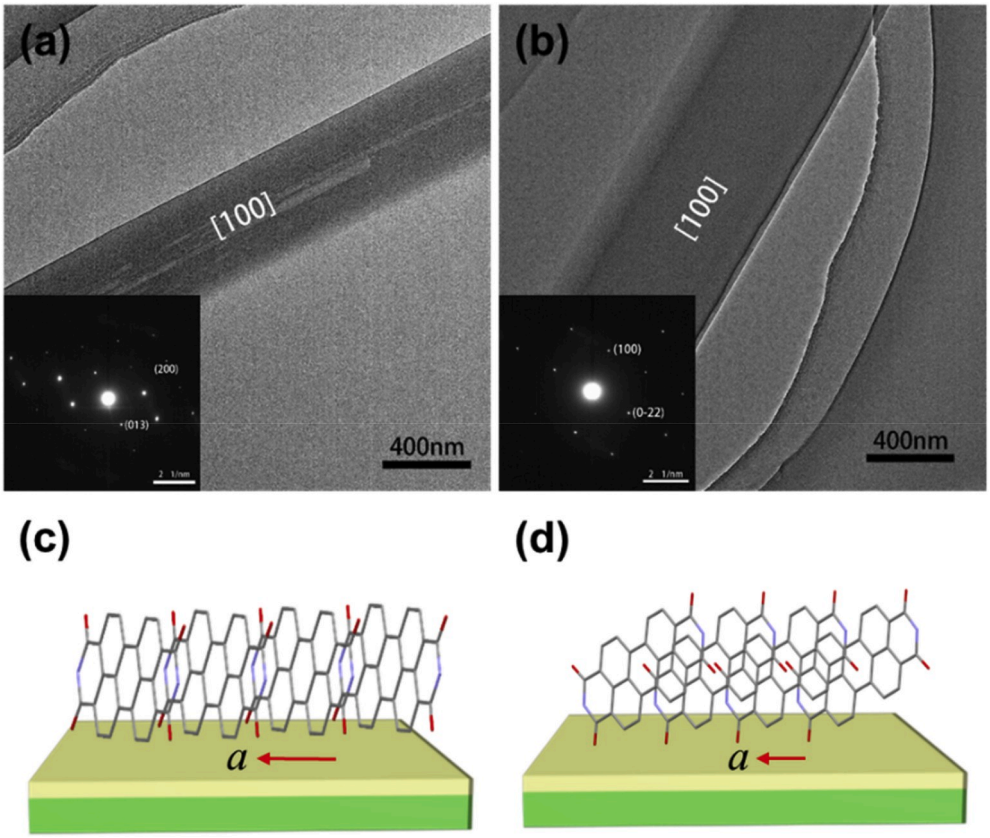

Fig. 4. TEM images and (illustration) SAED patterns of as-prepared (a) nanowires and (b) nanoribbons, respectively. The growth mode of (c) α phase and (d) β phase nanostructures on the substrates. In order to show the stacking pattern more clearly, we removed the benzene ring and other unnecessary groups, and only retained the core skeleton in this pattern.

2.3. Nanowire and nanoribbon preparation

Solutions of 4FPEPTC dissolved in chlorobenzene at concentrations of 0.02 mg/ml and 0.2 mg/ml were first prepared, which were sonicated for 1 h and then heated at 185 °C until all components were dissolved completely. A drop of the solutions was drop-casted onto the SiO_2/Si substrate in a nitrogen-fulled glovebox followed by 60 °C thermal annealing for 1 h, and then kept overnight. Ultimately, sub-millimetric nanostructures were observed on the substrate.

2.4. Device fabrication

The SiO_2/Si substrate was heavily doped *n*-type Si wafer with a 500 nm thick SiO_2 layer and a capacitance of 7.5 nF cm^{-2}. Bare substrates were successively cleaned with pure water, piranha solution (H_2SO_4: H_2O_2 = 2:1), pure water, and pure 2-propanol. Nanostructures-based *n*-type organic field-effect transistors (OFETs) with a bottom-gate top-contact (BGTC) configuration were fabricated via thermally evaporating gold electrodes (0.3 Å/s, 7×10^{-4} Pa) through a copper grid, with the channel length (L) of ~20 μm.

2.5. Characterization

The as-prepared nanostructures were characterized by Optical microscope (OM, Olympus BX3M-KMA-S), Powder X-ray diffraction (XRD, Rigaku D/Max2500/PC), UV–visible absorption spectrum (UV–vis spectra, LAMBDA 35), Atomic force microscopy (AFM, Bruker Dimension Icon), Scanning electron microscope (SEM, S4800) Transmission electronic microscopy (TEM, HITACHI HT7700) and corresponding selected-area electron diffraction (SAED, HITACHI HT7700). The data were collected at 113 K and the structure was resolved by the direct method and refined by the full-matrix least-squares method on F^2. The electrical characteristics of the devices were measured with a Keithley 4200 SCS semiconductor parameter analyzer under ambient conditions. The field-effect mobilities, threshold voltage and current on−off ratios were calculated in the saturation regime from the transfer plot of V_G versus I_{DS} and using the following equation

$$I_{DS} = \frac{WC_i}{2L}\mu(V_{GS} - V_{th})^2 \quad (1)$$

where W and L refer to the channel length and width, respectively, μ represents the electron mobility, V_{th} is the threshold voltage, and C_i is the capacitance per unit area of the SiO_2 gate dielectric (7.5×10^{-8} F/cm^2).

Characterization of light response performance is based on testing the device under the ambient environment with polychromatic white incident light (polychromatic white light via a halogen lamp source) at a power of 274.2 mW/cm^2, which using the following equation

$$P = \frac{I_{light} - I_{dark}}{I_{dark}} \quad (2)$$

$$R = \frac{I_{light} - I_{dark}}{S \cdot P_i} \quad (3)$$

where I_{light} is the drain current under illumination, I_{dark} is the drain current in the dark, P is the photosensitivity of device, S is the effective device area, P_i is the incident light intensity and R is the photoresponsivity of device.

2.6. Theoretical calculation details

All calculations were performed with G09 at the level of B3LYP/6-

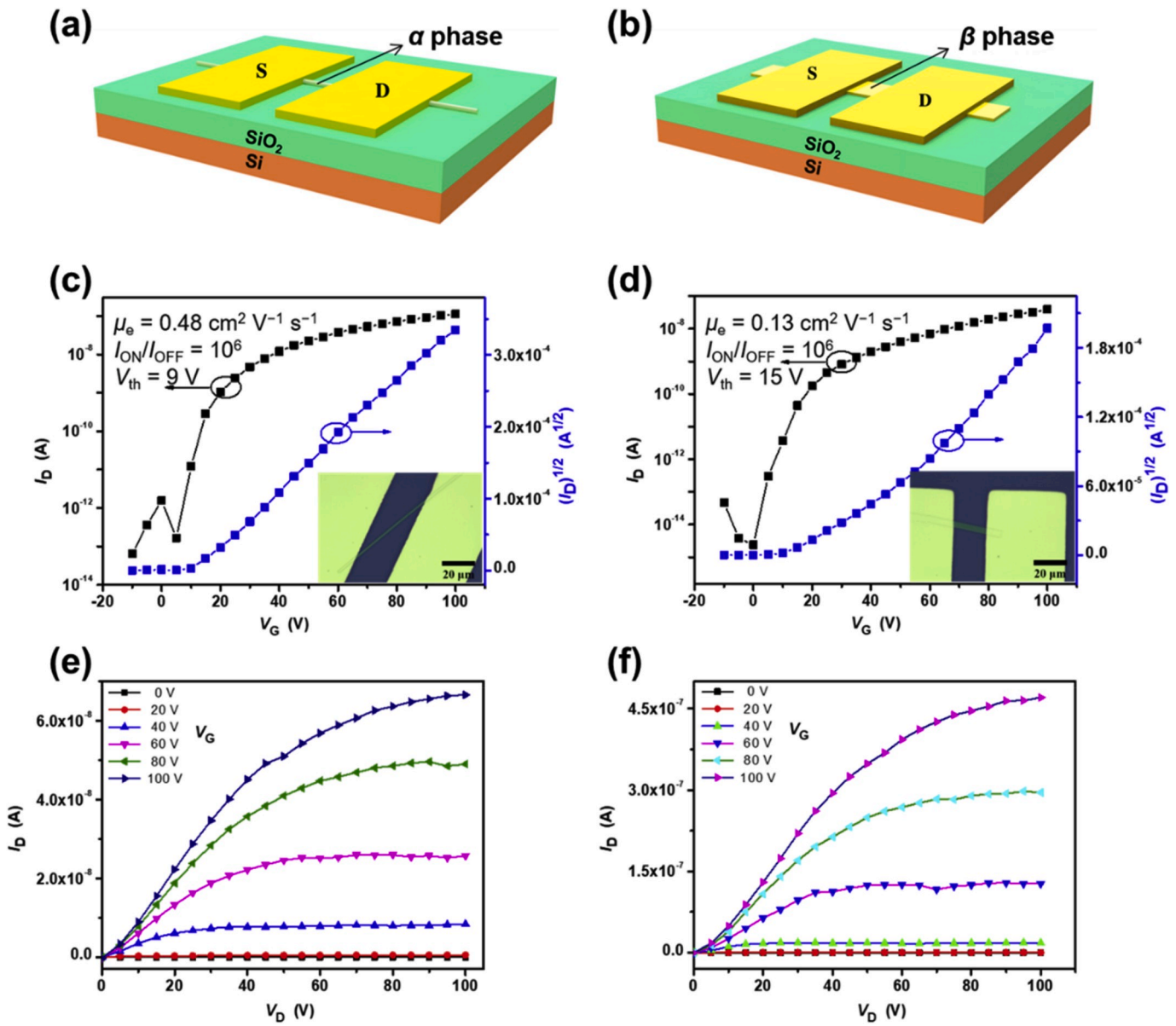

Fig. 5. OFET schematic diagrams based on (a) α phase and (b) β phase crystals. (c, d) Typical transfer ($V_{DS} = 100$ V) and (e, f) output characteristics of the single (c, e) nanowire and (d, f) nanoribbon device. Insets in (c, d) show one individual microcrystal device based on 4FPEPTC.

311G**. Charge transfer rate was calculated by Marcus theory:

$$\omega_{ij} = \frac{2\pi}{h}\frac{J_{ij}^2}{\sqrt{4\pi\lambda_{ij}\kappa_B T}} exp\left[-\frac{(\Delta E_{ij} - \lambda_{ij})^2}{4\lambda_{ij}\kappa_B T}\right] \quad (4)$$

3. Results and discussion

The two 4FPEPTC crystals were individually prepared via a simple solution cooling approach, wire-like α phase crystals grew from the relative low concentration chlorobenzene solution and ribbon-like β phase crystals from the high concentration solution observed at the bottom of the bottles. Both polymorphic crystals were further characterized by single-crystal X-ray diffraction. The crystallographic data of two crystal polymorphs are summarized in Table S1. The α phase crystal possessed a triclinic unit cell and belonged to the *P-1* space group with unit cell parameters of $a = 4.6839(2)$ Å, $b = 9.9616(5)$ Å, $c = 18.0176(9)$ Å, $\alpha = 77.647(2)°$, $\beta = 87.251(2)°$, and $\gamma = 81.372(2)°$. It was evident that α phase molecules adopted one-dimensional face-to-face stacking mode with $\pi-\pi$ distance of ~3.466 Å along *a*-axis in this crystal (Fig. 1a and b), ensuring good orbital overlap between the neighboring molecules which could enable strong electronic coupling, good charge transport in this phase was expected along the π-π interaction direction. Short contacts of H–F bonds determined to be ~2.602 Å between the neighboring molecule tails were observed. In addition, H–O hydrogen bonds between the nearby planar backbones were also brought into the construction architecture (Fig. S1). The β phase crystal possessed a triclinic unit cell and belongs to the *P-1* space group with unit cell parameters of $a = 4.8692(16)$ Å, $b = 14.636(5)$ Å, $c = 20.819(8)$ Å, $\alpha = 71.205(10)°$, $\beta = 88.115(10)°$, and $\gamma = 84.085(10)°$. Compared to the α phase, the β-4FPEPTC molecules had a denser $\pi-\pi$ stacking pattern along the *a*-axis with the closest interplanar distance of 3.402 Å, indicating strong molecular interactions (Fig. 1c and d). The obvious difference in the arrangement between these two crystals lied in the increased non-bond interactions (Fig. S2), hydrogen-bonding short contacts existed between one molecule with the adjacent six ones which were not in the same plane, and we believed that this reduced the dimension extension from 1D needle to the quasi-2D ribbon. The large supersaturation was supposed to lead to increased multiple

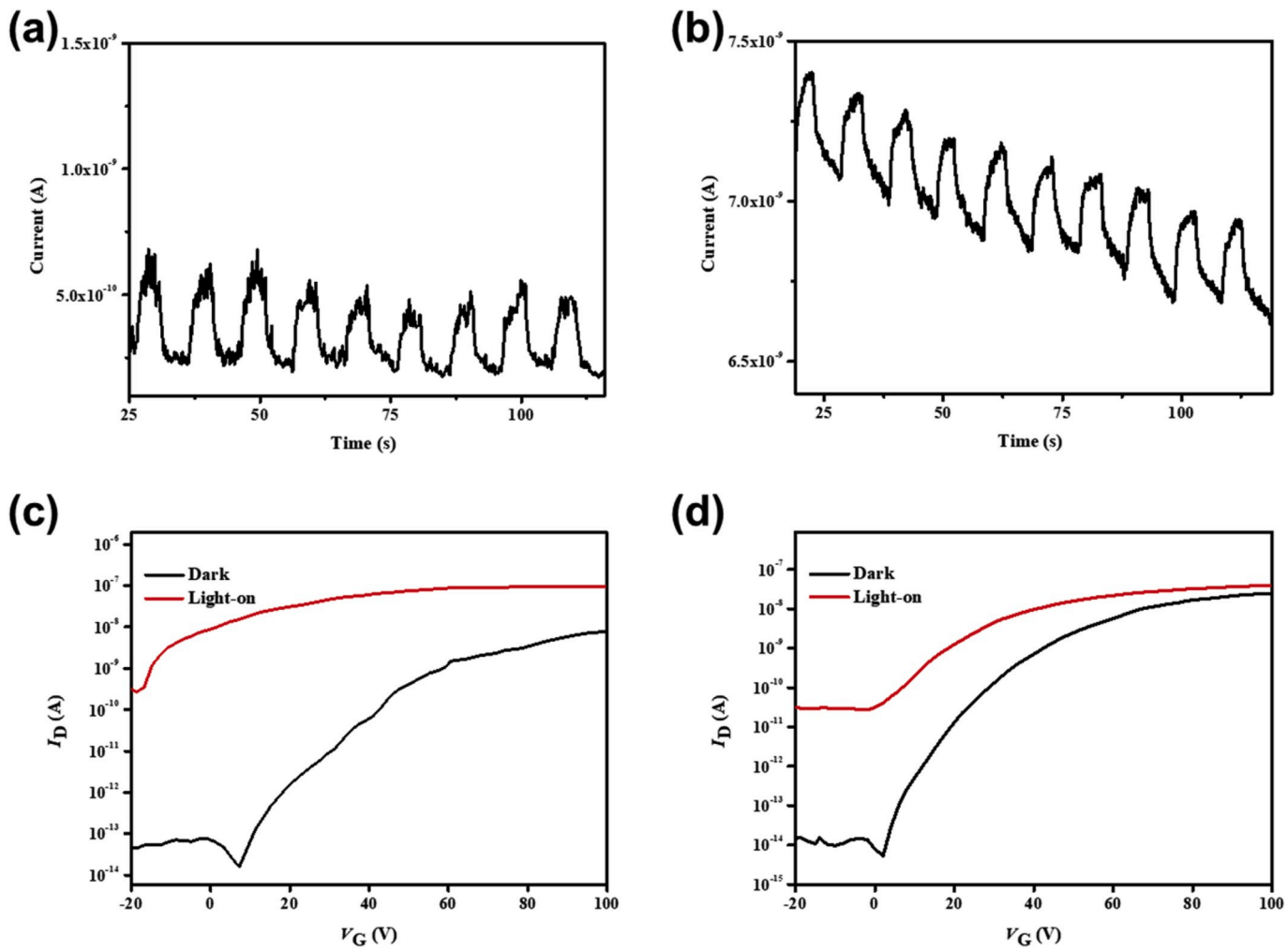

Fig. 6. Photoswitching behaviors of the (a) nanowire and (b) nanoribbon transistor to pulsed polychromatic white incident light ($V = 20$V). (c, d) I_{DS}–V_{GS} transfer curves for a 4FPEPTC nanostructure OFET acquired in dark and under light illumination at $V_{DS} = 100$ V.

intermolecular forces of this PDI derivative under the large molecular concentration environment and rapid crystal growth process. According to the solid-state UV–vis absorption spectra, we can see that there are absorption bands at ~492 nm and 529 nm for both crystal forms (Fig. S3).

Two different crystal-phase based micro/nanostructures could be easily obtained by drop-casting chlorobenzene solutions with different concentrations. A dilute chlorobenzene solution (0.02 mg/mL) was used to produce 1D nanowires (α phase, Fig. 2a and Fig. S4) with hundreds of micrometers in length, several hundred nanometers in width and dozens to hundreds of nanometers in height. On the contrary, ribbon-like crystalline nanostructures (β phase) of DPNDI were prepared from the relative high concentration solution (0.2 mg/ml), with dozens of micrometers in length, hundreds of nanometers in height and several micrometers in width (Fig. 2b and Fig. S5). The corresponding AFM (Fig. 2c and d) and SEM (Fig. 2e and f) images unveiled the smooth surfaces and uniform morphology.

The structures of the as-prepared 4FPEPTC-based nanostructures were further detected by powder X-ray diffraction (XRD), both of which corresponded to their own bulk crystal data (Fig. 3). Both nanowires and nanoribbons exhibited sharp Bragg reflections, suggesting the good crystallinity. For the nanowires (α phase), the XRD pattern showed intense peaks at 11.05°, which could be indexed as (0–11). According to the crystal data, it can be determined that α phase crystal grows perpendicularly along the π-conjugated backbones rather than the alkyl chain side. In the case of nanoribbon morphology (β phase), the strong peak at 8.61° and 17.65° was indexed as (00–2) and (00–4), respectively, indicating the molecules leaning on the substrate with one half part contact.

The transmission electron microscopy (TEM) and selected area electron diffraction (SAED) patterns were conducted for fully investigation, as shown in Fig. 4a and b. No changes observed in different regions of the same nanostructure in SAED images illustrated the good single-crystallinity. Furthermore, it revealed that both nanowire and micro/nanoribbon grew along [100] direction, induced by the strong π-π interactions. Combined with the powder X-ray diffraction (XRD) patterns, the overall growth mode was as shown in Fig. 4c and d, preferred to lie or lean on the substrates, followed by the inherent structure change.

To explore how polymorphism affect the charge transport property, we constructed the microcrystal-based field-effect transistors with the bottom-gate top-contact geometry (Fig. 5a and b). Au source/drain electrodes were thermally evaporated onto the in-situ prepared nanowires/ribbons via a copper grid as the shadow mask. All the characterizations were conducted in air condition. Typical transfer and output characteristics of α phase single crystal devices are shown in Fig. 5c and e, which exhibit well-saturated n-type performance. According to the calculation formula of mobility in saturation region (Equation (1)), over 50 individual devices were measured and they exhibited an average μ_e (electron mobility) of 0.32 $cm^2\ V^{-1}\ s^{-1}$ and V_{th} (Threshold voltage) of ~9 V. The highest electron transport mobility could reach up to 1.01 $cm^2\ V^{-1}\ s^{-1}$, with a high on/off ratio of 10^7. Meanwhile, the β phase

nanoribbon devices display an average and highest electron transport mobility up to 0.10 and 0.21 $cm^2 V^{-1} s^{-1}$ (Fig. 5d and f), respectively, which was much lower than that of the α phase nanowire. The results were inconsistent with our initial expectation resulting from the π-π distance and non-bonding interactions, the structure-property relationship will be discussed later on. Additionally, time-dependent photoswitching behaviors of the 4FPEPTC nanostructure were recorded where the polychromatic white light illumination was chosen to detect.

Fig. 6a and b show the photoresponse behavior of a micro/nanocrystal device as a function of time, both nanowire and nanoribbon devices exhibit relatively stable photoswitching reaction ($V_{SD} = 20$ V and $V_G = 0$ V). Nanoribbon devices are more vulnerable with more rough currents to the voltage bias than nanowire devices, which may be probably affected by the scattering centers from the substrate, charge-trapping surface states, and crystalline imperfection. Fig. 6c and d illustrate transfer characteristics of top-contact 4FPEPTC nanostructure transistors upon irradiation with polychromatic white light or dark at an applied drain voltage bias of 100 V. Under light irradiation, the observed transistor photoresponse consists a dramatic increase of both OFF and ON currents and a negative shift in V_T, indicating that such device is easy to turn on. This is probably due to the elimination of trap sites by the photogenerated charge carriers. In addition, according to equations (2) and (3), we calculated the photoresponsivity (R) and photosensitivity (P) of the two polymorphic devices (Fig. S6) [41,42]. The α phase device has P and R of 9.78×10^5 and 800 mA/W, respectively, which are hundreds or even thousands of times higher than the corresponding values of the β phase device ($P = 7.53 \times 10^3$ and $R = 0.54$ mA/W). Therefore, the polymorphism induced arrangement diversity has a great influence on photosensitive behavior of the device, opens avenues for their functional applications in optoelectronic devices.

We then conducted the quantum simulations to understanding how the molecular packing affect their electronic properties in this n-type system [43], the electronic couplings were calculated under the level of B3LYP/6-311G**, which was implemented in Gaussian 09. Fig. S7 presents the main charge-transport pathways for electrons predicted in α and β phase crystals. It is noteworthy that the electronic coupling along the π-π stacking direction of 7–8 is about at least 6 times higher than that in other directions, reaching up to 116.36 meV. No efficient electronic coupling in other planes is found. Thus, this pathway was believed to be the dominating electron transporting route, known as the nanowire growth direction. As for the β phase crystal, along the crystal long axis direction of 19–21 (π-π stacking direction, 36.22 meV) was also much higher than that in other directions, noting that dimers in the other plane exhibited very small couplings (less than 1 meV). Obviously, these differences in molecular packing structures play an important role in their both charge transport features. Finally, we also calculated their mobility (α and β phase crystals) based on Marcus theory (Equation (4)) and kinetic Monte Carlo simulations [44]. The theoretical mobility of α phase and β phase device is 0.23 $cm^2 V^{-1} s^{-1}$, and 0.01 $cm^2 V^{-1} s^{-1}$, respectively. The calculated electron mobility in α phase was higher than that of β phase of 4FPEPTC, which was in agreement with the experimental results.

4. Conclusion

We report the preparation of two crystalline forms of n-type F-substituted PDI derivative by a simple and efficient solution method (supersaturated solution cooling with different concentrations). Particularly, we believe that the increased supersaturation prevents one dimensional $\pi-\pi$ stacking direction to form a nanowire structure as the molecules crystallize, resulting in a dimension extended nanoribbon packing mode with more non-bonding interactions. The OFETs based on single-crystalline 4FPTCDI nanowires and nanoribbons were further fabricated, and found that nanowire structures (α phase structure) possessed larger electron mobility up to 1 $cm^2 V^{-1} s^{-1}$ and much higher photosensitivity. Theoretical calculations show that the β phase crystal prefer absolute 1D charge transport path although the quasi-2D packing, and lower charge carrier mobility was supposed compared to α phase polymorph. In summary, this polymorphism tuning by simple solution method provides us a powerful approach for the deep study of the structure-property and exploring of the functional organic optoelectronic materials.

Declaration of competing interest

The authors declare no conflicts of interest.

Acknowledgements

This work was supported by the National Natural Science Foundation of China (21602113 and 61774087), and Research Foundation for Advanced Talents of Nanjing University of Posts and Telecommunications. G. L thanks the European Union's Horizon 2020 research and innovation programme under the Marie-Sklodowska-Curie grant agreement (No. 791207).

Appendix A. Supplementary data

Supplementary data to this article can be found online at https://doi.org/10.1016/j.orgel.2020.105777.

Author contributions

All authors contributed to this manuscript. X.L., H.X., Y.Z., J.Z., W. W., Y.M., G.L. came up with the outline. Y.Z. made the theoretical calculations. H.X. wrote the final manuscript.

References

[1] R. Li, W. Hu, Y. Liu, D. Zhu, Micro- and nanocrystals of organic semiconductors, Acc. Chem. Res. 43 (2010) 529–540.
[2] Z.L. Wang, The new field of nanopiezotronics, Mater. Today 10 (2007) 20–28.
[3] P. Gu, Z. Wang, G. Liu, H. Yao, Z. Wang, Y. Li, J. Zhu, S. Li, Q. Zhang, Synthesis, full characterization, and field effect transistor behavior of a stable pyrene-fused N-heteroacene with twelve linearly annulated six-membered rings, Chem. Mater. 29 (2017) 4172–4175.
[4] H. Xu, Y. Zhou, J. Zhang, J. Jin, G. Liu, Y. Li, R. Ganguly, L. Huang, W. Xu, D. Zhu, W. Huang, Q. Zhang, Polymer-assisted single crystal engineering of organic semiconductors to alter electron transport, ACS Appl. Mater. Interfaces 10 (2018) 11837–11842.
[5] P. He, Z. Tu, G. Zhao, Y. Zhen, H. Geng, Y. Yi, Z. Wang, H. Zhang, C. Xu, J. Liu, X. Lu, X. Fu, Q. Zhao, X. Zhang, D. Ji, L. Jiang, H. Dong, W. Hu, Tuning the crystal polymorphs of alkyl thienoacene via solution self-assembly toward air-stable and high-performance organic field-effect transistors, Adv. Mater. 27 (2015) 825–830.
[6] Y.Q. Zheng, Z.F. Yao, T. Lei, J.H. Dou, C.Y. Yang, L. Zou, X. Meng, W. Ma, J. Y. Wang, J. Pei, Unraveling the solution-state supramolecular structures of donor-acceptor polymers and their influence on solid-state morphology and charge-transport properties, Adv. Mater. 29 (2017) 1072–1079.
[7] G.E. Purdum, N. Yao, A. Woll, T. Gessner, R.T. Weitz, Y.L. Loo, Understanding polymorph transformations in core-chlorinated naphthalene diimides and their impact on thin-film transistor performance, Adv. Funct. Mater. 26 (2016) 2357–2364.
[8] C. Wang, H. Dong, W. Hu, Y. Liu, D. Zhu, Semiconducting π-conjugated systems in field-effect transistors: a material odyssey of organic electronics, Chem. Rev. 112 (2012) 2208–2267.
[9] Y. Diao, K.M. Lenn, W.Y. Lee, M.A. Blood-Forsythe, J. Xu, Y. Mao, Y. Kim, J. A. Reinspach, S. Park, A. Aspuru-Guzik, G. Xue, P. Clancy, Z. Bao, S.C. Mannsfeld, Understanding polymorphism in organic semiconductor thin films through nanoconfinement, J. Am. Chem. Soc. 136 (2014) 17046–17057.
[10] H. Zhang, K. Liu, K.Y. Wu, C.Y. Chen, R. Deng, X. Li, H. Jin, S. Li, S.S.C. Chuang, C. Wang, Y. Zhu, Hydrogen-bonding-mediated solid-state self-assembled isoepindolidiones (isoEpi) crystal for organic field-effect transistor, J. Phys. Chem. C 122 (2018) 5888–5895.
[11] J.H. Kim, M.W. Choi, W.S. Yoon, S. Oh, S.H. Hong, S.Y. Park, Structural and electronic origin of bis-lactam-based high-performance organic thin-film transistors, ACS Appl. Mater. Interfaces 11 (2019) 8301–8309.
[12] Y. Ma, Y. Zhou, J. Jin, W. Wang, X. Liu, H. Xu, J. Zhang, W. Huang, Pentacene derivative/DTTCNQ cocrystals: alkyl-confined mixed heterojunctions with molecular alignment and transport property tuning, Chem. Sci. 10 (2019) 11125–11129.

[13] D. Gentili, M. Gazzano, M. Melucci, D. Jones, M. Cavallini, Polymorphism as an additional functionality of materials for technological applications at surfaces and interfaces, Chem. Soc. Rev. 48 (2019) 2502–2517.
[14] H. Chung, Y. Diao, Polymorphism as an emerging design strategy for high performance organic electronics, J. Mater. Chem. C 4 (2016) 3915–3933.
[15] O.D. Jurchescu, D.A. Mourey, S. Subramanian, S.R. Parkin, B.M. Vogel, J. E. Anthony, T.N. Jackson, D.J. Gundlach, Effects of polymorphism on charge transport in organic semiconductors, Phys. Rev. B 80 (2009), 085201.
[16] J. Chen, M. Shao, K. Xiao, A.J. Rondinone, Y.L. Loo, P.R. Kent, B.G. Sumpter, D. Li, J.K. Keum, P.J. Diemer, J.E. Anthony, O.D. Jurchescu, J. Huang, Solvent-type-dependent polymorphism and charge transport in a long fused-ring organic semiconductor, Nanoscale 6 (2014) 449–456.
[17] J.C. Sorli, Q. Ai, D.B. Granger, K. Gu, S. Parkin, K. Jarolimek, N. Telesz, J. E. Anthony, C. Risko, Y.-L. Loo, Impact of atomistic substitution on thin-film structure and charge transport in a germanyl-ethynyl functionalized pentacene, Chem. Mater. 31 (2019) 6615–6623.
[18] G. Giri, E. Verploegen, S.C. Mannsfeld, S. Atahan-Evrenk, D.H. Kim, S.Y. Lee, H. A. Becerril, A. Aspuru-Guzik, M.F. Toney, Z. Bao, Tuning charge transport in solution-sheared organic semiconductors using lattice strain, Nature 480 (2011) 504–508.
[19] A. Brillante, I. Bilotti, R.G. Della Valle, E. Venuti, M. Masino, A. Girlando, Characterization of phase purity in organic semiconductors by lattice-phonon confocal Raman mapping: application to pentacene, Adv. Mater. 17 (2005) 2549–2553.
[20] L. Li, Q. Tang, H. Li, X. Yang, W. Hu, Y. Song, Z. Shuai, W. Xu, Y. Liu, D. Zhu, An ultra closely π-stacked organic semiconductor for high performance field-effect transistors, Adv. Mater. 19 (2007) 2613–2617.
[21] K. Vasseur, B.P. Rand, D. Cheyns, K. Temst, L. Froyen, P. Heremans, Correlating the polymorphism of titanyl phthalocyanine thin films with solar cell performance, J. Phys. Chem. Lett. 3 (2012) 2395–2400.
[22] R. Pfattner, M. Mas-Torrent, I. Bilotti, A. Brillante, S. Milita, F. Liscio, F. Biscarini, T. Marszalek, J. Ulanski, A. Nosal, M. Gazicki-Lipman, M. Leufgen, G. Schmidt, L. W. Molenkamp, V. Laukhin, J. Veciana, C. Rovira, High-performance single crystal organic field-effect transistors based on two dithiophene-tetrathiafulvalene (DT-TTF) polymorphs, Adv. Mater. 22 (2010) 4198–4203.
[23] J. Li, S. Chen, Z. Wang, Q. Zhang, Pyrene-fused acenes and azaacenes: synthesis and applications, Chem. Rec. 16 (2016) 1518–1530.
[24] H. Chung, D. Dudenko, F. Zhang, G. D'Avino, C. Ruzie, A. Richard, G. Schweicher, J. Cornil, D. Beljonne, Y. Geerts, Y. Diao, Rotator side chains trigger cooperative transition for shape and function memory effect in organic semiconductors, Nat. Commun. 9 (2018) 278.
[25] H. Geng, X. Zheng, Z. Shuai, L. Zhu, Y. Yi, Understanding the charge transport and polarities in organic donor-acceptor mixed-stack crystals: molecular insights from the super-exchange couplings, Adv. Mater. 27 (2015) 1443–1449.
[26] G. Lu, X. Kong, P. Ma, K. Wang, Y. Chen, J. Jiang, Amphiphilic (phthalocyaninato) (porphyrinato) europium triple-decker nanoribbons with air-stable Ambipolar OFET performance, ACS Appl. Mater. Interfaces 8 (2016) 6174–6182.
[27] M. Zangoli, M. Gazzano, F. Monti, L. Maini, D. Gentili, A. Liscio, A. Zanelli, E. Salatelli, G. Gigli, M. Baroncini, F. Di Maria, Thermodynamically versus kinetically controlled self-assembly of a naphthalenediimide-thiophene derivative: from crystalline, fluorescent, n-type semiconducting 1D needles to nanofibers, ACS Appl. Mater. Interfaces 11 (2019) 16864–16871.
[28] Z.-P. Fan, X.-Y. Li, G.E. Purdum, C.-X. Hu, X. Fei, Z.-F. Shi, C.-L. Sun, X. Shao, Y.-L. Loo, H.-L. Zhang, Enhancing the thermal stability of organic field-effect transistors by electrostatically interlocked 2D molecular packing, Chem. Mater. 30 (2018) 3638–3642.
[29] Z. Wang, F. Yu, J. Xie, J. Zhao, Y. Zou, Z. Wang, Q. Zhang, Insights into the control of optoelectronic properties in mixed-stacking charge-transfer complexes, Chem. Eur J., 10.1002/chem.201904901.
[30] H. Jiang, X. Yang, Z. Cui, Y. Liu, H. Li, W. Hu, Y. Liu, D. Zhu, Phase dependence of single crystalline transistors of tetrathiafulvalene, Appl. Phys. Lett. 91 (2007) 123505.
[31] J. Zhang, J. Jin, H. Xu, Q. Zhang, W. Huang, Recent progress on organic donor–acceptor complexes as active elements in organic field-effect transistors, J. Mater. Chem. C 6 (2018) 3485–3498.
[32] G.R. Desiraju, Crystal engineering: from molecule to crystal, J. Am. Chem. Soc. 135 (2013) 9952–9967.
[33] A.O.F. Jones, B. Chattopadhyay, Y.H. Geerts, R. Resel, Substrate-induced and thin-film phases: polymorphism of organic materials on surfaces, Adv. Funct. Mater. 26 (2016) 2233–2255.
[34] J. Zhang, G. Liu, Y. Zhou, G. Long, P. Gu, Q. Zhang, Solvent accommodation: functionalities can Be tailored through Co-crystallization based on 1:1 coronene-F4TCNQ charge-transfer complex, ACS Appl. Mater. Interfaces 9 (2017) 1183–1188.
[35] L.A. Stevens, K.P. Goetz, A. Fonari, Y. Shu, R.M. Williamson, J.-L. Brédas, V. Coropceanu, O.D. Jurchescu, G.E. Collis, Temperature-mediated polymorphism in molecular crystals: the impact on crystal packing and charge transport, Chem. Mater. 27 (2015) 112–118.
[36] H. Xu, J. Jin, J. Zhang, P. Sheng, Y. Li, M. Yi, W. Huang, Investigation of self-assembly and charge-transport property of one-dimensional PDI8-CN2 nanowires by solvent-vapor annealing, Materials 12 (2019) 438–447.
[37] G. Horowitz, F. Kouki, P. Spearman, D. Fichou, C. Nogues, X. Pan, F. Garnier, Evidence for n-type conduction in a perylene tetracarboxylic diimide derivative, Adv. Mater. 8 (1996) 242–245.
[38] D. Khim, Y. Xu, K.J. Baeg, M. Kang, W.T. Park, S.H. Lee, I.B. Kim, J. Kim, D.Y. Kim, C. Liu, Y.Y. Noh, Large enhancement of carrier transport in solution-processed field-effect transistors by fluorinated dielectric engineering, Adv. Mater. 28 (2016) 518–526.
[39] R. Schmidt, J.H. Oh, Y.-S. Sun, M. Deppisch, A.-M. Krause, K. Radacki, H. Braunschweig, M. Konemann, P. Erk, Z. Bao, F. Wurthner, High-performance air-stable n-channel organic thin film transistors based on halogenated perylene bisimide semiconductors, J. Am. Chem. Soc. 131 (2009) 6215–6228.
[40] A.S. Molinari, H. Alves, Z. Chen, A. Facchetti, A.F. Morpurgo, High electron mobility in vacuum and ambient for PDIF-CN2 single-crystal transistors, J. Am. Chem. Soc. 131 (2009) 2462–2463.
[41] X. Liu, E.K. Lee, D.Y. Kim, H. Yu, J.H. Oh, Flexible organic phototransistor array with enhanced responsivity via metal-ligand charge transfer, ACS Appl. Mater. Interfaces 8 (2016) 7291–7299.
[42] G. Wang, K. Huang, Z. Liu, Y. Du, X. Wang, H. Lu, G. Zhang, L. Qiu, Flexible, low-voltage, and n-type infrared organic phototransistors with enhanced photosensitivity via interface trapping effect, ACS Appl. Mater. Interfaces 10 (2018) 36177–36186.
[43] H. Xu, Y.-C. Zhou, X.-Y. Zhou, K. Liu, L.-Y. Cao, Y. Ai, Z.-P. Fan, H.-L. Zhang, Molecular packing-induced transition between ambipolar and unipolar behavior in dithiophene-4,9-dione-containing organic semiconductors, Adv. Funct. Mater. 24 (2014) 2907–2915.
[44] Y. Zhou, W. Deng, H. Zhang, Phonon-electron coupling and tunneling effect on charge transport in organic semi-conductor crystals of Cn-BTBT, J. Chem. Phys. 145 (2014) 2768–2788.